Cortical circuit activity underlying sleep slow oscillations and spindles

Niels Niethard[a,1], Hong-Viet V. Ngo[a,b], Ingrid Ehrlich[c,d,2], and Jan Born[a,c,1]

[a]Institute of Medical Psychology and Behavioral Neurobiology, University of Tübingen, 72076 Tübingen, Germany; [b]School of Psychology, University of Birmingham, B15 2TT Birmingham, United Kingdom; [c]Center for Integrative Neuroscience, University of Tübingen, 72076 Tübingen, Germany; and [d]Hertie Institute for Clinical Brain Research, University of Tübingen, 72076 Tübingen, Germany

Edited by Gyorgy Buzsáki, New York University Neuroscience Institute, New York, NY, and approved August 16, 2018 (received for review April 5, 2018)

Slow oscillations and sleep spindles are hallmarks of the EEG during slow-wave sleep (SWS). Both oscillatory events, especially when co-occurring in the constellation of spindles nesting in the slow oscillation upstate, are considered to support memory formation and underlying synaptic plasticity. The regulatory mechanisms of this function at the circuit level are poorly understood. Here, using two-photon imaging in mice, we relate EEG-recorded slow oscillations and spindles to calcium signals recorded from the soma of cortical putative pyramidal-like (Pyr) cells and neighboring parvalbumin-positive interneurons (PV-Ins) or somatostatin-positive interneurons (SOM-Ins). Pyr calcium activity was increased more than threefold when spindles co-occurred with slow oscillation upstates compared with slow oscillations or spindles occurring in isolation. Independent of whether or not a spindle was nested in the slow oscillation upstate, the slow oscillation downstate was preceded by enhanced calcium signal in SOM-Ins that vanished during the upstate, whereas spindles were associated with strongly increased PV-In calcium activity. Additional wide-field calcium imaging of Pyr cells confirmed the enhanced calcium activity and its widespread topography associated with spindles nested in slow oscillation upstates. In conclusion, when spindles are nested in slow oscillation upstates, maximum Pyr activity appears to concur with strong perisomatic inhibition of Pyr cells via PV-Ins and low dendritic inhibition via SOM-Ins (i.e., conditions that might optimize synaptic plasticity within local cortical circuits).

sleep | calcium imaging | slow oscillation | spindle | inhibition

Mammalian slow-wave sleep (SWS) is characterized by two major EEG oscillatory events (the slow oscillation and the sleep spindle). The slow oscillation, also considered a neurophysiological substrate of EEG slow-wave activity, is characterized by widespread synchronized changes in the membrane potential of cortical neurons between hyperpolarization during the slow oscillation downstate and depolarization during the slow oscillation upstate, occurring at frequencies between 0.1 and 4 Hz (1, 2). Neural silence characterizing the slow oscillation downstate pertains to excitatory neurons as well as inhibitory interneurons (3, 4). The slow oscillation is primarily generated within cortical networks, where it can occur in the absence of thalamocortical input, with major participation of layer 5 neurons (5–7). Nevertheless, in natural conditions, thalamic inputs substantially contribute to the occurrence of cortical slow oscillation upstates (8). Slow oscillations often show propagation patterns as waves traveling from anterior to posterior cortical areas (9–11).

Sleep spindles are characterized by waxing and waning oscillatory field potentials in a frequency range between 7 and 15 Hz and with a duration of 0.5–3 s (1). Within this frequency band in the human EEG, fast and slow spindles can be discriminated, which differ in topography and possibly also in their function (12, 13). Sleep spindles are generated in intrathalamic circuits comprising GABAergic neurons within the nucleus reticularis thalami and in collaterals of glutamatergic thalamocortical projection neurons, with these projections also mediating their propagation to widespread neocortical regions (14–16), where they reach both excitatory and inhibitory cells. The initiation and termination of spindles critically depend on corticothalamic feedback (17, 18). The generation of spindles is driven by the depolarizing upstate of the neocortical slow oscillation such that they tend to nest in the beginning phase of the cortical slow oscillation upstate (2).

There is convergent evidence that slow oscillations, as well as spindles, contribute to the consolidation of memory during sleep and underlying cortical synaptic plasticity mediating this memory effect (19–23). The slow oscillation is thought to convey primarily global processes of synaptic downscaling and renormalization (24), although it might concurrently contribute to long-term potentiation and upscaling of synapses in local cortical circuits (25). Spindles and associated neural firing patterns have been shown to promote cortical synaptic long-term potentiation (23, 26, 27). The consolidation of memory during sleep likely originates from the repeated reactivation of respective neural ensemble activity in hippocampal as well as neocortical networks (28–30). Such reactivations occur preferentially during the upstate of the cortical slow oscillation. In fact, the depolarizing upstate of the slow oscillation appears to drive neural memory reactivations and thalamocortical spindles in parallel (31–33). In this framework, slow oscillations co-occurring with spindles have been proposed to be particularly effective in forming long-term memory and in regulating underlying synaptic plasticity (34–36).

Significance

Slow oscillations and spindles are hallmarks of the EEG during slow-wave sleep. They are thought to support memory consolidation, particularly in instances where the faster spindle nests into the "upstate" of a slow oscillation. Using two-photon and wide-field imaging, we recorded calcium transients from distinct populations of cortical excitatory and inhibitory neurons during sleep in mice. Compared with spindles or slow oscillations occurring in isolation, events where spindles nested in a slow oscillation upstate were indeed accompanied by a unique pattern of calcium activity where high pyramidal cell activity appears to concur with high perisomatic inhibition through parvalbumin-positive interneurons and with low dendritic inhibition through somatostatin-positive interneurons. These conditions might foster dendritic plasticity.

Author contributions: N.N. and J.B. designed research; N.N. performed research; I.E. contributed new reagents/analytic tools; N.N. and H.-V.V.N. analyzed data; and N.N. and J.B. wrote the paper.

The authors declare no conflict of interest.

This article is a PNAS Direct Submission.

[1]To whom correspondence may be addressed. Email: niels.niethard@uni-tuebingen.de or jan.born@uni-tuebingen.de.

[2]Present address: Institute of Biomaterials and Biomolecular Systems, Department of Neurobiology, University of Stuttgart, 70569 Stuttgart, Germany.

This article contains supporting information online at www.pnas.org/lookup/suppl/doi:10.1073/pnas.1805517115/-/DCSupplemental.

Published online September 12, 2018.

Here, we aimed to directly link calcium activity, also as a factor that has been considered to eventually enable the neural plasticity underlying memory formation during SWS (37) in the mouse cortex, to EEG measures of slow oscillations and spindles, reflecting synchronized membrane potential oscillations in cortical networks. Two-photon imaging was used to assess calcium activity before, during, and after solitary slow oscillations and spindles, and spindles co-occurring with slow oscillation upstates, in pyramidal-like (Pyr) cells and neighboring parvalbumin-positive interneurons (PV-Ins) and somatostatin-positive interneurons (SOM-Ins) representing the major populations of excitatory and inhibitory neurons, respectively, in cortical circuits. We find that solitary slow oscillation upstates and spindles are accompanied by increased Pyr calcium activity. Inhibitory regulation during the slow oscillation appears to be conveyed mainly by SOM-Ins, which show strongly increased calcium activity in the beginning of the slow oscillation downstate and also a transient increase in the beginning of the slow oscillation upstate, whereas inhibitory PV-In activity is dominant during spindles. Notably, spindles nesting in the slow oscillation upstate are accompanied by maximal increases in Pyr activity, while inhibitory PV-In activity is maintained at the same high level as during solitary spindles and SOM-In activity is low.

Results

We investigated the activity of layer 2/3 PV-Ins and SOM-Ins and of neighboring putative Pyr cells during slow oscillations and spindles occurring in isolation and during co-occurring slow oscillation-spindle events during SWS (Fig. 1 *A*, *C*, and *D*). For this purpose, we identified PV-Ins and SOM-Ins in PV-Cre and SOM-Cre transgenic mice by Cre-dependent expression of tdTomato and assessed the calcium signal as a proxy for cellular activity by panneuronal expression of GCaMP6f (cf. ref. 38) (Fig. 1 *B* and *D*). Calcium activity of all three cell types was compared during a 5-s time window lasting from 2 s before to 3 s after the negative slow oscillation half-wave peak and the spindle onset, respectively. Activity between −3 and −2 s before the negative slow oscillation half-wave peak and spindle onset, respectively, was used as a baseline. Average calcium activity during this baseline interval did not differ between solitary slow oscillations, solitary spindles, and spindles co-occurring with slow oscillations ($P > 0.23$). Three different frequency bands were used to analyze spindles: slow spindles (7–10 Hz), fast spindles (11–15 Hz), and broad-band spindles (7–15 Hz). As no major differences were found, we focused on broad-band 7–15-Hz spindles as characterized in previous reports (3, 15, 17).

SI Appendix, Table S1 summarizes basic features of the analyzed slow oscillations and spindles. With our criteria for slow oscillation and spindle detection (*Materials and Methods*), we detected a total of 18,931 solitary slow oscillations in seven animals (PV-Cre animals: 8,062, SOM-Cre animals: 10,869), 1,311 solitary spindles (PV-Cre animals: 557, SOM-Cre animals: 754) and 1,092 spindles co-occurring with slow oscillation upstates (PV-Cre: 451, SOM-Cre: 641). Across imaging sessions and animals, mean slow oscillation duration (0.61 ± 0.008 s vs. 0.61 ± 0.01 s) and amplitude (0.26 ± 0.01 mV vs. 0.27 ± 0.01 mV) were closely comparable between slow oscillations and slow oscillations co-occurring with spindles. Whereas the duration of solitary spindles was slightly shorter than for spindles co-occurring with slow oscillations (0.71 ± 0.01 s vs. 0.77 ± 0.01 s; $P < 0.001$), interevent intervals (3.26 ± 0.2 s vs. 3.63 ± 0.1 s) and peak frequencies (12.14 ± 0.04 Hz vs. 12.09 ± 0.04 Hz) did not differ between the spindle types ($P > 0.1$; Fig. 1*E*).

Activity of Pyr Cells, PV-Ins, and SOM-Ins During Slow Oscillations and Spindles. All three cell types of interest showed distinct modulations of their activity during solitary slow oscillations and spindles, and during slow oscillation-spindle events (Fig. 2 *A* and *B*). To assess the temporal dynamics of cell activity during the slow oscillation, the slow oscillation cycle was divided into four phases (Fig. 2*C*, *Top*): (*i*) a positive-to-negative "transition" phase (0.32 to −0.00 s before a negative half-wave peak), (*ii*) the "down" phase (−0.00 to +0.16 s), the "up" phase (+0.32 to +0.48 s), and an "after" phase (+0.54–3 s). In solitary slow oscillations, the transition phase was hallmarked by a distinct increase in SOM-In activity paralleled by a significant decrease in PV-In activity (both $P < 0.01$ with reference to baseline activity; Fig. 2 *B* and *C*). Increases in Pyr cell activity during the transition phase were not significant. During the subsequent down phase, we observed significantly reduced activity, on average, across all three cell types [in percent signal change value ($\Delta F/F$) $\times 10^{-3}$: −6.3 ± 0.5, −7.1 ± 0.7, and −6.1 ± 0.6 for Pyr cells, PV-Ins, and SOM-Ins, respectively; all $P < 0.001$]. In the up phase, putative Pyr cells and SOM-Ins displayed significant increases in activity ($P < 0.01$), averaging +2.8 ± 0.5 and +1.7 ± 0.7 (in $\Delta F/F \times 10^{-3}$), respectively. For SOM-Ins, this increase was restricted to the initial part of the up phase (Fig. 2*B*). By contrast, PV-In activity during the up phase did not differ from baseline. In the after phase, all cell types displayed significantly reduced activity (all $P < 0.01$). Exploratory principal component analyses (PCAs) confirmed a predominant inhibitory control via SOM-Ins rather than PV-Ins during the slow oscillation. This analysis identified one component starting with the transition phase and extending over the whole slow oscillation, with component scores in the opposite direction for SOM-Ins and PV-Ins (*SI Appendix*, Fig. S1).

During solitary spindles [+0.00 to +1.00 s with reference to spindle onset ("during")], PV-Ins showed distinctly increased activity (on average, by +10.1 ± 3.0 $\Delta F/F \times 10^{-3}$; $P < 0.001$). For putative Pyr cells, a similar increase did not reach significance (Fig. 2*B*). By contrast, SOM-In activity did not differ from baseline (Fig. 2*C*). After solitary spindles [+1.00 to +3.00 s with reference to spindle onset (after)], activity of SOM-Ins was decreased, compared with baseline levels ($P < 0.05$). PCA confirmed an opposing modulation of PV-In and SOM-In cells, reflecting high PV-In activity and low SOM-In activity, for the major component covering the whole spindle range (*SI Appendix*, Fig. S1).

To examine how the temporal dynamics in cell activity during a slow oscillation were modified by a spindle nesting in its up phase, we compared patterns during solitary slow oscillations and slow oscillation-spindle events (Fig. 2*C*). For all three cell types, activity did not significantly differ between solitary slow oscillations and slow oscillation-spindle events before (transition phase) and during the slow oscillation down phase. During the subsequent up phase, co-occurring spindles consistently enhanced Pyr cell activity more than threefold ($P < 0.01$) and PV-In activity more than 20-fold ($P < 0.01$), but did not change SOM-In activity (Fig. 2*C*). Additional analyses revealed that for both Pyr cells and PV-Ins, the duration of calcium transients, as assessed per cell, during the up phase was longer for slow oscillation-spindle events compared with calcium transients observed during solitary slow oscillations ($P < 0.01$). In the after phase of slow oscillations, when spindles co-occurred with slow oscillations, we observed a reduction in activity for putative Pyr cells and PV-Ins ($P < 0.01$) compared with solitary slow oscillations, but not for SOM-Ins. ANOVA across all slow oscillation phases confirmed significant co-occurring/solitary × phase interactions for all three cell types (Pyr: $F = 8.2$, $P < 0.001$; PV-In: $F = 10.7$, $P < 0.001$; SOM-In: $F = 4.1$, $P < 0.01$).

After comparing solitary slow oscillations and slow oscillations co-occurring with spindles, we likewise assessed whether the presence of a slow oscillation upstate changed the dynamics of cell activity seen during solitary spindles (Fig. 2*C*, *Right*). This analysis confirmed that the activity of putative Pyr cells was more than threefold higher during a spindle that nested in a slow oscillation upstate than during a solitary spindle ($P < 0.05$),

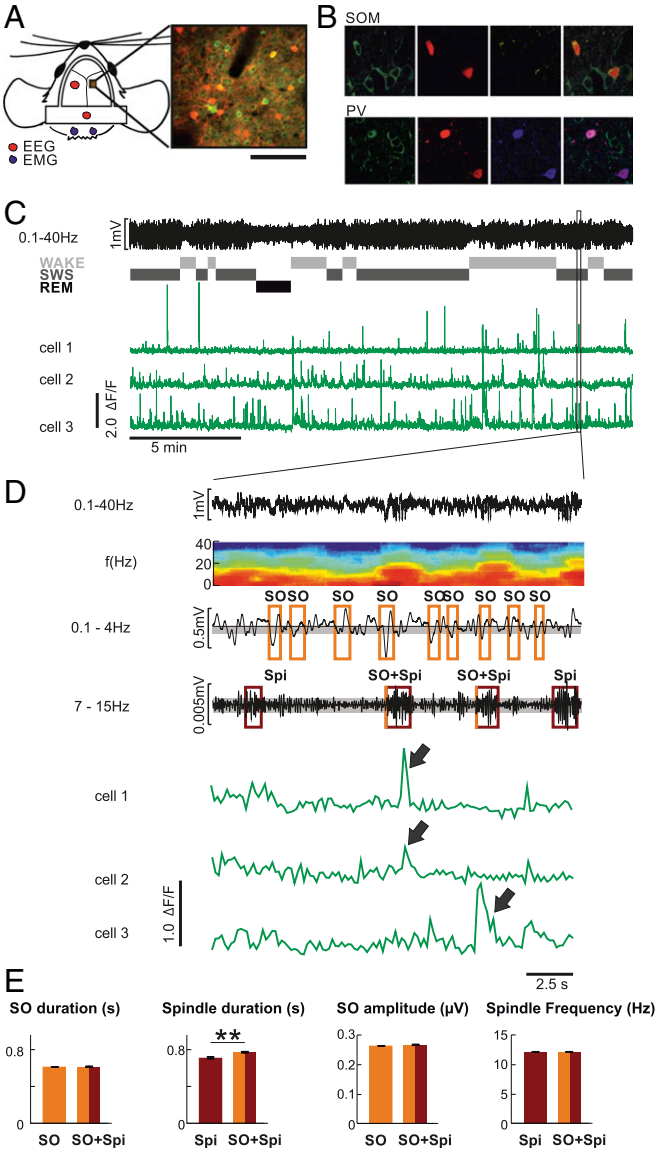

Fig. 1. Simultaneous EEG recording and two-photon calcium imaging. (*A*, *Left*) Illustration of EEG and electromyography (EMG) electrode positions and of the imaging window for the two-photon experiments. (*A*, *Right*) Example frame from one SOM-Cre animal. (Scale bar: 100 μm.) (*B*) Fluorescence image of GCaMP6f (green) and td-tomato–positive interneurons (red; *Top*, SOM-Cre; *Bottom*, PV-Cre) and immunohistochemical staining (yellow, SOM; blue, PV). (*C*) Example EEG trace (from a parietal electrode) and, underneath, corresponding classification of sleep stages [wake, SWS, rapid eye movement (REM) sleep] and example calcium activity traces from three individual putative Pyr cells. The frame marks the interval magnified in *D*. (*D*, *Top*) Zoomed-in EEG trace (from a parietal electrode) and, underneath, the corresponding time-frequency plot. For detection of slow oscillation(s) (SO), the EEG signal was filtered between 0.1 and 4.0 Hz. An SO was identified in the EEG when (*i*) the distance between consecutive positive-to-negative zero crossings was between 0.4 and 2 s, (*ii*) the amplitude of the negative half-wave peak in this interval exceeded 0.66 SD (gray-shaded range) from the mean of all identified intervals in a recording session, and (*iii*) the difference in amplitude between the negative and succeeding positive peak was greater than 2/3 of the average negative-to-positive peak amplitude for all identified intervals in a recording session. Spindle(s) (Spi) were detected when the amplitude of the filtered EEG signal (7–15 Hz) was greater than 1.5 SDs from the mean (gray-shaded range) amplitude during a recording session for at least 0.5 s. (*D*, *Bottom*) Example fluorescence traces (ΔF/F) from three individual putative Pyr cells during the same time interval. Note the synchronous activity of cells 1 and 2 during the first Spi co-occurring with an SO and of cell 3 during the second Spi co-occurring with an SO (arrows). (*E*) Summary of SO and Spi properties (mean duration, mean SO amplitude, mean Spi frequency across all animals and all recorded events), separately for isolated SO and Spi and for SO co-occurring with Spi (SO + Spi). $^{**}P < 0.01$, for pairwise comparison (corresponding results for each animal are shown in *SI Appendix*, Table S1).

whereas activity of PV-Ins during these two types of spindles was at a high but comparable level during solitary and nested spindles. Also, the after phase of spindles was characterized by enhanced Pyr cell activity when the spindle had occurred during a slow oscillation compared with solitary spindles [$F = 5.1$, $P < 0.05$ for co-occurring/solitary main effect in an ANOVA across both phases (i.e., during and after the spindle)].

To examine to what extent scattered fluorescence from the neuropil contaminated the fluorescence signal from the cell soma, we repeated the analyses using ΔF/F values that were neuropil-corrected. In this approach, calcium events were detected whenever the signal within a frame exceeded 2 SDs of the median neuropil-corrected fluorescence signal of the cell (*Materials and Methods*). This analysis revealed temporal dynamics of calcium event rates during solitary spindles, slow oscillations, and slow oscillation-spindle events, which are summarized in *SI Appendix*, Fig. S2. These control analyses rule out the possibility that the results concerning uncorrected ΔF/F signal from the three neuron subpopulations of interest reported above are substantially contaminated by scattering dendritic fluorescence.

Overall, these findings indicate the existence of specific mechanisms of circuit regulation for slow oscillations and spindles. On one side, slow oscillations are characterized by enhanced SOM-In activity, which precedes the initial negative slow oscillation half-wave peak and seems to also counterregulate the distinct increase in Pyr cell activity during the slow oscillation upstate. On the other side, during spindles, increased PV-In activity appears to counterregulate the increase in Pyr cell activity. The co-occurrence of a slow oscillation upstate with a spindle produces a maximum increase in Pyr cell activity in the presence of high levels of PV-In activity and low levels of SOM-In activity.

Wake-Active Versus Wake-Inactive Neurons. Previous studies have revealed that cell activity dynamics differ depending on the cell's activity during wakefulness (38–40). To investigate whether the wake activity level affected cell-specific calcium activity during slow oscillations and spindles, we compared, separately for each of the three cell types of interest, fluorescence signals between the 20% of cells (fifth quintile) that were most active during wakefulness and the 20% of cells (first quintile) that were least active during wake phases (*SI Appendix*, Fig. S3).

This comparison revealed that wake-inactive SOM-In cells displayed a stronger modulation of calcium activity by slow oscillations and spindles than the wake-active SOM-In cells (*SI Appendix*, Fig. S3). For putative Pyr and PV-In cells, the direct comparisons between wake-active and wake-inactive cells did not reach significance, which might partly reflect the enhanced signal variability in these subsamples.

Fluorescence Signal Correlates with EEG Signal During Slow Oscillations and Spindles. To clarify the relationship between fluorescence intensity and EEG signal amplitude during slow oscillations and spindles, we calculated Pearson's correlation coefficients between respective measures. Only a few survived Bonferroni corrections for multiple testing. For slow oscillations, correlations were stronger for the negative-to-positive peak amplitude measure than for the other amplitude measures (negative half-wave and positive half-wave peak amplitudes) and slightly higher for slow oscillations co-occurring with spindles than for solitary slow oscillations. Correlations between $r = 0.12$ and $r = 0.09$ ($P < 0.01$) were found between the slow oscillation negative-to-positive amplitude and

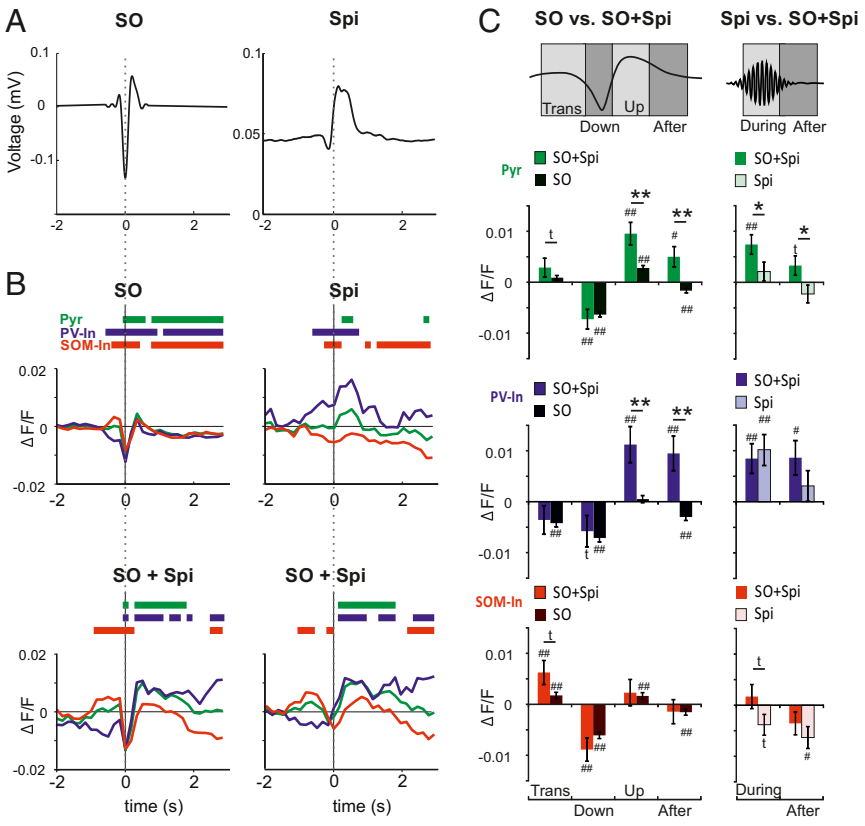

Fig. 2. Distinct modulation of calcium activity during slow oscillation and spindle. (*A*, *Left*) Grand average (across all events from all animals) of the EEG signal (filtered between 0.1 and 4 Hz) during slow oscillation(s) (SO) time-locked to the negative SO half-wave peak (0 s). (*A*, *Right*) Grand average of the rms of EEG spindle (Spi) signal (7–15 Hz) time-locked to Spi onset (0 s). (*B*) Mean ΔF/F signals for putative Pyr cells (green), PV-Ins (blue), and SOM-Ins (red) during solitary SO (*Top Left*) and solitary Spi (*Top Right*) and during SO co-occurring with Spi (SO + Spi), time-locked to a negative SO half-wave peak (*Bottom Left*) and to Spi onset (*Bottom Right*). Bars on top indicate significance ($P < 0.05$) with reference to a baseline (−3 to −2 s) set to zero. Average traces across all events from all animals are indicated. (*C*, *Left*) Comparison of mean (±SEM) ΔF/F signals between solitary SO and SO + Spi events for the positive-to-negative transition phase (Trans; −0.32 to −0.00 s, with reference to the SO negative half-wave peak = 0 s), the down phase (−0.00 to 0.16 s), the up phase (0.32–0.48 s), and the following after phase (0.54–3 s). (*C*, *Right*) Comparisons between mean (±SEM) ΔF/F signals between solitary Spi and SO + Spi events for the phase during the acute Spi (0–1 s with reference to Spi onset set to 0 s) and the after phase (1–3 s). $^{**}P < 0.01$, $^{*}P < 0.05$, and $^{t}P < 0.1$ for pairwise comparisons between solitary events and SO + Spi events respectively. $^{\#\#}P < 0.01$, $^{\#}P < 0.05$, and $^{t}P < 0.1$ for difference from baseline activity (−3 to −2 s).

the ΔF/F signal of Pyr cells and SOM-Ins, respectively, during the transition, down, and up phases of slow oscillations co-occurring with spindles, with overall highest coefficients for correlations with the signal during the up phase.

Analyses of spindles revealed somewhat higher correlations (Fig. 3). The ΔF/F signal of putative Pyr cells showed significant positive correlations with spindle power, with this correlation being more robust for spindles co-occurring with slow oscillations ($r = 0.19$, $P < 0.001$) than for solitary spindles ($r = 0.12$, $P < 0.001$). Moreover, for spindles co-occurring with slow oscillations, this correlation was significantly ($P < 0.001$) stronger for wake-active Pyr cells (fifth quintile; $r = 0.27$, $P < 0.001$) than for wake-inactive cells (first quintile; $r = 0.12$, $P < 0.001$). On the other side, wake-inactive SOM-Ins (first quintile) showed stronger correlations between ΔF/F signals and spindle power than wake-active SOM-Ins during spindles co-occurring with slow oscillations ($r = 0.18$, $P < 0.001$ vs. $r = 0.04$ $P = 0.27$; $P < 0.001$ for difference between coefficients).

We also calculated pairwise correlations of ΔF/F signals within the populations of putative Pyr cells, PV-In cells, and SOM-In cells, as well as between Pyr cells and the two inhibitory cell populations (*SI Appendix*, Fig. S4). Generally, these correlations were small ($r < 0.15$), and their distribution did not provide evidence for the presence of highly correlated subgroups of cells accompanying the occurrence of slow oscillations or spindles.

Cortical Topography of Calcium Activity During Slow Oscillations and Spindles. To characterize the cortical topography of slow oscillation and spindle-related changes in calcium activity, we used wide-field imaging of the dorsal surface of the cortex in mice (Fig. 4 *A* and *B*). This technique provides calcium signals with high temporal resolution (50–60 frames per second) and, additionally, broader fields of view covering cortical areas in ranges of square centimeters (38, 41). The cortical surface of transgenic animals expressing a genetically encoded calcium indicator (GCaMP6f) in almost all cortical Pyr cells (CaMKII-positive cells) was monitored. To investigate the topographical distribution of calcium activity during sleep spindles and slow oscillations, we compared grand averages (across all events from all animals) of f_{norm} signals in 36 regions of interest (ROIs) during solitary slow oscillations, solitary spindles, and slow oscillations co-occurring with spindles, with the EEG events detected in recordings from either the left frontal cortex or the left occipital cortex. To characterize anterior and posterior cortical activities, and for the respective statistical comparisons, activity was averaged across four frontal and four occipital target ROIs (Fig. 4*A*).

During solitary slow oscillations, calcium signal showed a widespread and significant reduction during the down phase regardless of whether the slow oscillation was identified in the frontal or occipital EEG channel ($P < 0.05$ for analysis of target ROIs, with reference to baseline levels −3 to −2 s before the negative half-wave peak; Fig. 4*C* and *SI Appendix*, Fig. S5). This decrease was followed by a transient increase in calcium signal in the beginning of the slow oscillation up phase, which did not significantly differ from baseline, however. Solitary spindles detected in the frontal EEG channel were associated with significantly increased calcium signal in the anterior target ROIs, which was succeeded by a widespread reduction in calcium signal persisting for more than 3 s after the spindle had ceased ($P < 0.01$). This reduction in signal was likewise significant for solitary spindles identified in the occipital EEG ($P < 0.01$ for posterior target ROIs; *SI Appendix*, Fig. S5). Slow oscillations that co-occurred with a spindle were marked by a clear increase in calcium signal during the up phase, most pronounced over the anterior ROIs ($P < 0.01$). However, the mean f_{norm} signal amplitude during a 1-s interval starting with spindle onset did not significantly differ between solitary spindles and spindles that occurred during a slow oscillation upstate ($P > 0.1$). Like solitary slow oscillations, these slow oscillation-spindle events were associated with a widespread decrease in activity during the prior

down phase, and, like solitary spindles, they were followed by a widespread persisting suppression of activity ($P < 0.05$ across all target ROIs; *SI Appendix*, Figs. S5 and S6 show corresponding data for events detected in the occipital EEG channel).

Calcium activity associated with the slow oscillation revealed a systematic traveling from frontal to occipital cortical regions, such that reductions in activity during the negative half-wave peaked slightly earlier over frontal cortical areas than over posterior areas (Fig. 5 and Movie S1). This traveling was significant for both solitary slow oscillations and slow oscillation-spindle events (mean ± SEM delay between frontal ROIs 25–36 and occipital ROIs 1–12: 10.5 ± 1.7 ms; $P < 0.001$). No significant delay between hemispheres was found, and there were also no hints at a systematic traveling of spindle-associated changes in calcium activity.

We wanted to exclude the possibility that changes in fluorescence observed with GCaMP6f imaging are not reflecting calcium activity but are confounded by metabolic and/or blood flow changes, which can affect the intensity of the detected fluorescence signal. To this end, we measured fluorescence change in control animals expressing GFP within cortical layer 2/3, which is

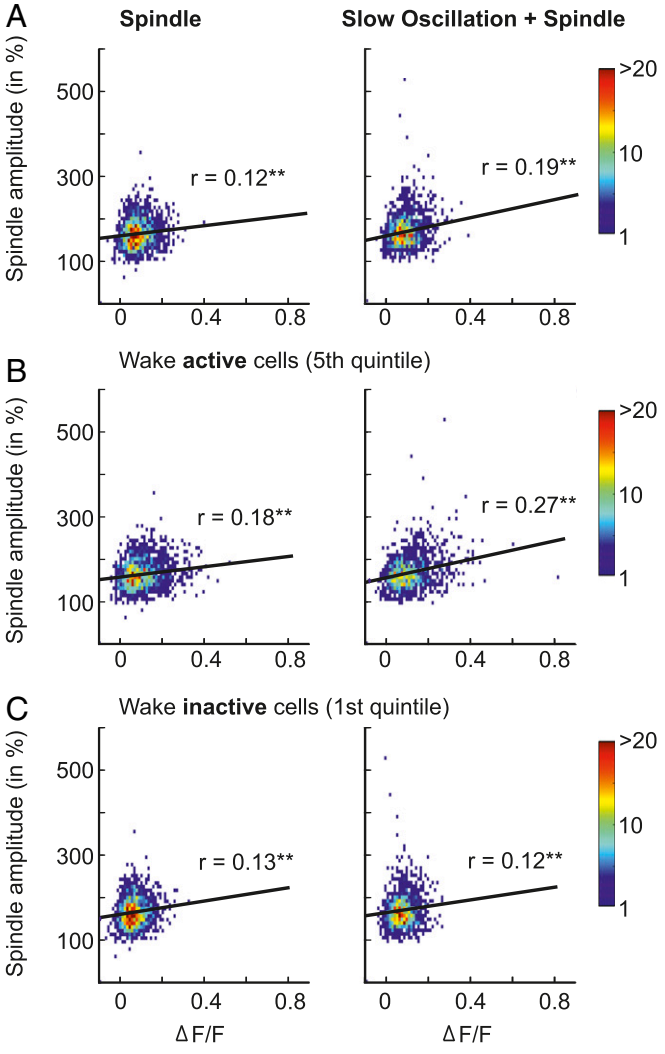

Fig. 3. Calcium activity of putative Pyr cells correlates with spindle amplitude. Density plots showing the correlation between activity of putative Pyr cells (mean ΔF/F across all cells for each event) and EEGs with 7–15-Hz spindle amplitude (normalized rms) for solitary spindles (*Left*) and spindles co-occurring with slow oscillations (*Right*). Results are shown separately for all Pyr cells (*A*), wake-active Pyr cells (*B*), and wake-inactive Pyr cells (*C*). $^{**}P < 0.001$.

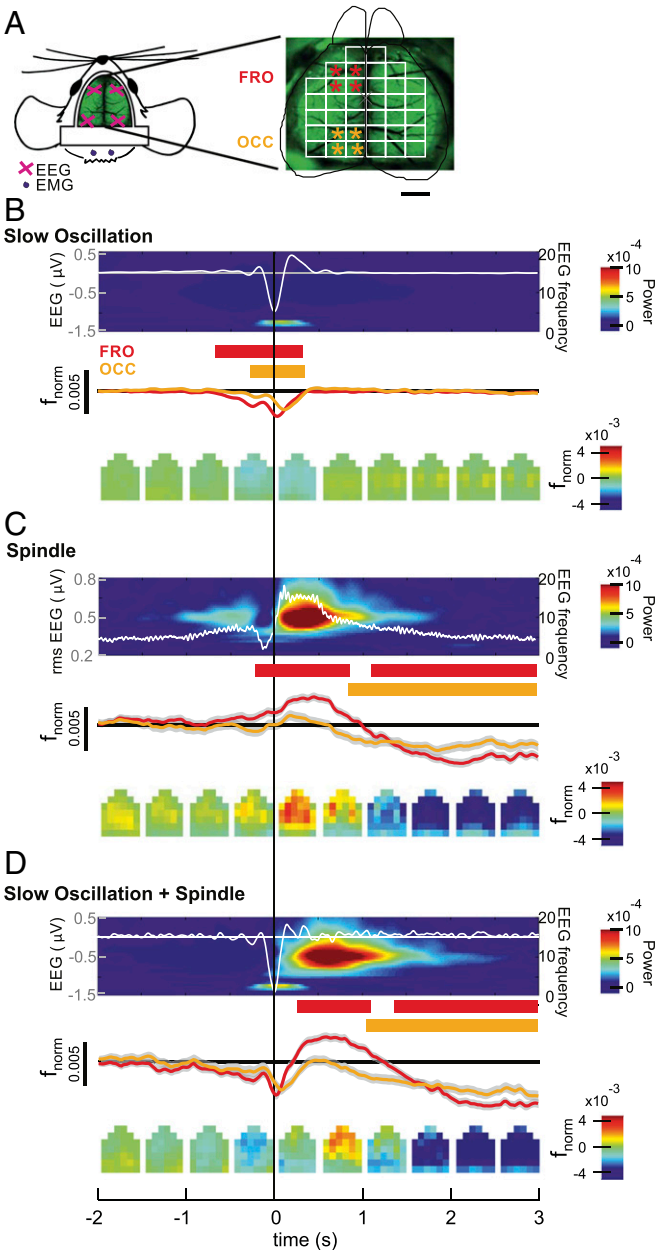

Fig. 4. Cortical topography of calcium activity during slow oscillation and spindle. (*A*) Schematic drawing of the wide field used for calcium imaging, positioning of electrodes for EEG (pink crosses), and electromyography (EMG) recordings (blue dots). (*Right*) Imaging window was divided into 36 ROIs. Asterisks mark ROIs used for statistical comparison of activity between anterior (red) and posterior (orange) regions. (Scale bar: 2 mm.) (*B*) Average EEG signal for solitary slow oscillations (*Top*; from left frontal cortical recordings, white line overlaying average time-frequency plot with color-coded power) together with average (±SEM) calcium activity (f_{norm}) across the four designated anterior (red) and posterior (orange) cortical regions (*Middle*). Averages are time-locked to the negative half-wave peak of the slow oscillation (0 s). Intervals with significant changes in calcium activity ($P < 0.01$, relative to the baseline interval from −3 to −2 s) are indicated in red [for anterior ROIs (FRO)] and orange bars [for posterior ROIs (OCC)]. (*Bottom*) Topographic changes of calcium activity in all 36 ROIs (f_{norm}, color-coded) for subsequent 500-ms time windows. (*C* and *D*) Corresponding data for solitary spindles (Spindle) and slow oscillations co-occurring with spindles (Slow oscillation + Spindle). Note that for solitary spindles, the average EEG signal (overlaying the corresponding EEG time-frequency plot) shows the rms amplitude and averaging is time-locked to the spindle onset. Average traces are shown across events from four animals (total: $n =$ 9,472, $n = 706$, and $n = 770$, for solitary slow oscillations, solitary spindles, and slow oscillations co-occurring with spindles, respectively; corresponding results for EEG events identified in occipital recordings are shown in *SI Appendix*, Fig. S5).

not a calcium-dependent fluorescent protein (*Materials and Methods*). As expected, these animals showed neither the acute decrease and increase in calcium signal accompanying the slow oscillation downstate and upstate nor an acute increase in calcium signal during spindles ($P < 0.001$ for all relevant comparisons with the experimental GCaMP6f animals).

Discussion

Using calcium imaging in the naturally sleeping brain, our study provides evidence that the slow oscillations and spindles of SWS are characterized by a specific balance between the activity of excitatory and specific inhibitory neurons within cortical circuits. We find that the slow oscillation upstates and, to a far lesser extent, spindles are accompanied by an increase in calcium activity of putative Pyr cells. The excitatory drive during the slow oscillation appears to be mainly countered by inhibitory activity of SOM-Ins showing distinct increases in the beginning of the downstate and also transiently in the beginning of the upstate. By contrast, inhibitory activity during spindles is primarily conveyed by increased activity of PV-Ins. Importantly, when spindles co-occur with the slow oscillation upstate, Pyr calcium activity reaches a maximum in the presence of high levels of PV-In activity and low levels of SOM-In activity.

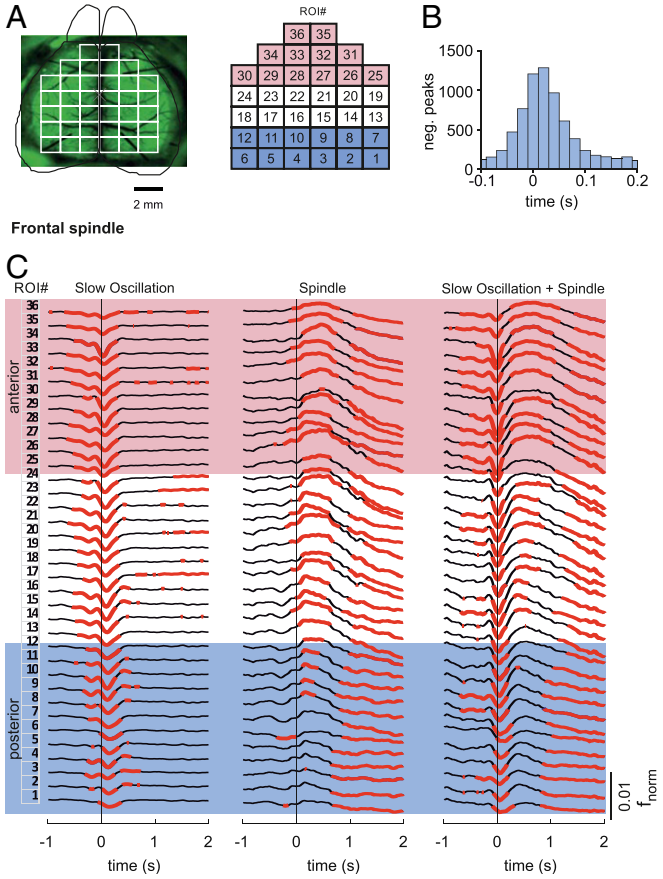

Fig. 5. Slow oscillation-associated calcium signal travels from anterior to posterior cortex. (*A*) Illustration of the 36 cortical ROIs used for wide-field imaging experiments. The red-shaded area indicates anterior ROIs (25–36), and the blue-shaded area indicates posterior ROIs (1–12). (*B*) Histogram showing the distribution of the temporal delays of slow oscillation negative (neg.) half-wave peaks defined in the f_{norm} signal between frontal ROIs and occipital ROIs. Only slow oscillation events were included in this analysis, where the minimum of the f_{norm} signal was associated with the slow oscillation half-wave peak exceeding a critical threshold for both anterior and posterior regions (with the threshold defined by 0.66 SD from the mean activity of the filtered 0.1–4-Hz signal). (*C*) Calcium activity for 36 cortical ROIs using wide-field imaging during solitary slow oscillations (*Left*), solitary spindles (*Center*), and slow oscillations co-occurring with spindles (*Right*, Slow Oscillation + Spindle). The red-shaded area indicates anterior ROIs, and the blue-shaded area indicates posterior ROIs. The numbering of ROIs is indicated in *A*. Average traces across four animals (total: $n = 9472$, $n = 706$, and $n = 770$ for solitary slow oscillations, solitary spindles, and slow oscillations co-occurring with spindles, respectively) are indicated. Averaging is time-locked (0 s) to the negative half-wave peak of slow oscillation and spindle onset, respectively. EEG events were detected in the frontal EEG channel (corresponding results for EEG events detected in occipital recordings are shown in *SI Appendix*, Fig. S6). The red-marked calcium signal indicates intervals of significantly ($P < 0.05$) enhanced or reduced activity (with reference to activity during the baseline interval from −3 to −2 s).

Our results, revealing an increase in SOM-In calcium activity at the transition into the slow oscillation downstate as well as at the transition into the upstate, shed light on the regulation underlying the emergence of the cortical slow oscillation. The slow oscillation downstate is considered a disfacilitatory state (1, 42), which is confirmed by the present findings indicating a general decrease in the activity of excitatory Pyr cells as well as inhibitory PV-Ins or SOM-Ins during the downstate. However, what triggers the downstate, and what explains its high synchrony across cortical columns, has been unclear for a long time. Based on studies of slice preparations of the rodent entorhinal cortex, an involvement of slow GABA(B) receptors as well as D1-like dopaminergic receptors has been suggested (43, 44). Comparisons of local field potentials in mice lacking glutamate decarboxylase 67 in either SOM-Ins or PV-Ins provided the first hints that these cells might specifically contribute to the regulation of slow oscillation downstates and upstates (45). Strong electrophysiological evidence for the induction of the slow oscillation by distinct inhibitory activities has only recently been provided by Timofeev and coworkers (46). They found in natural sleeping cats that the slow oscillation downstate was preceded by a longer (100–300 ms) chloride-mediated inhibitory barrage that was likely mediated by long-range afferent inputs to inhibitory interneurons. The rather similar time course observed here for the increase in SOM-In activity preceding the slow oscillation downstate, together with findings that optogenetic stimulation of SOM-Ins can induce slow oscillations (47), speaks for a contribution of SOM-Ins in initialization of the slow oscillation downstate. This view is further supported by our observation that PV-In activity gradually decreased in the same time interval (i.e., before the downstate), as SOM-Ins are known to directly inhibit PV-Ins and a number of other cortical interneurons (48). The majority (~70%) of cortical SOM-In cells are Martinotti cells (49). They mainly target the apical dendrites of Pyr cells, where they regulate dendritic spike generation and synaptic integration in local networks of Pyr cells (50, 51). These properties make them a strong candidate for active induction of the slow oscillation downstate, as well as for regulating inhibitory control during the downstate-to-upstate transition, when their activity transiently increased.

Our finding that spindles are accompanied by a strong increase in PV-In calcium activity concurs with findings from electrophysiological studies. Not only do PV-In–like fast spiking cells show increased firing rates during spindles but firing is also in synchrony with the spindle oscillation (52, 53). On the other hand, Pyr cells do not show consistent increases in firing during spindles, even though they receive highly synchronized excitatory input. This picture of a predominant inhibitory regulation of spindles via feedforward or intracortical feedback inputs to PV-Ins agrees well with the present data of a distinct increase in PV-In activity accompanied by only a slight (but significant) increase in Pyr activity (54). Interestingly, at the same time, SOM-In activity was low, possibly reflecting inhibition of SOM-In via PV-In, thereby shifting Pyr inhibition from SOM-In–driven dendritic inhibition to PV-In–driven

perisomatic inhibition, which might favor dendritic synaptic plasticity (48, 55, 56).

Mainly based on computational models, it has been proposed that a massive intracellular increase in calcium in Pyr cells during spindles mediates persisting synaptic plastic changes underlying memory consolidation during sleep (37). This study provides evidence that calcium activity in cortical layer 2/3 Pyr is only slightly enhanced when spindles occur in isolation but becomes profoundly enhanced when the spindle occurs during a slow oscillation upstate, rendering such slow oscillation-spindle events a condition particularly fostering the consolidation of cortically represented memories (19, 36, 57).

Our data also uncover some of the underlying circuit conditions of the strong increase in Pyr activity during slow oscillation-spindle events, as it concurred with PV-In activity at levels as high as during solitary spindles, as well as with rather low SOM-In activity. The shift toward perisomatic inhibition by PV-Ins in the presence of low dendritic inhibition through SOM-Ins during slow oscillation-spindle events and solitary spindles probably enables local increases in calcium levels within dendrites by excitatory inputs. Such inputs might originate from reactivated memory representations in cortical and extracortical regions such as the hippocampus. As they are synchronized to the depolarizing slow oscillation upstate with a co-occurring spindle, they reach cortical Pyr cells in a time window of dendritic disinhibition, allowing for effective local calcium responses (31, 32, 35, 58). Indeed, in awake rats, dendritic encoding of sensory stimuli and associated increases in dendritic calcium levels were facilitated by increased perisomatic inhibition and simultaneously decreased inhibition through Martinotti cells (50). According to this scenario, low SOM-In activity during spindles nesting in slow oscillation upstates would play a permissive role for dendritic calcium activity, facilitating the induction of persisting plasticity at dendritic synapses in Pyr cells. Although this view is tentative, as we did not directly assess dendritic calcium activity, it concurs well with findings in awake mice showing that low SOM-In activity, in the presence of strong perisomatic inhibition of Pyr cells, facilitates dendritic synaptic plasticity upon encoding of motor memories in these cells (47, 55, 59). Moreover, during SWS, after motor memory encoding dendritic plasticity was shown to occur, as a consequence of reactivated representations, on select apical branches of Pyr cells (60) and dendritic calcium activity was found to be distinctly increased during spindles (54). Collectively, those and the present findings tempt one to propose that the constellation of low SOM-In–mediated dendritic inhibition, together with strong perisomatic inhibition of Pyr cells, is a general feature facilitating dendritic plasticity in postencoding wake conditions as well as during SWS, when newly encoded representations are reactivated in the presence of slow oscillation-spindle events (29, 31, 61).

Recent studies suggest that synaptic plastic changes during sleep depend on the prior activity of the involved neurons during wakefulness (62, 63). In the present study, differences between the most and least active cells during wakefulness were moderate overall and mainly found for inhibitory cells, but not for putative Pyr cells. The described dynamics in calcium activity, especially during spindles, appeared to be more pronounced in SOM-Ins and PV-Ins with the lowest wake activity than in those with highest wake activity, although direct comparisons between the cell clusters often failed to reach significance. This observation might be linked to electrophysiological findings indicating that cells with low firing activity are more likely involved in encoding specific memories (39). However, the greater dynamics in wake-inactive interneurons were observed independent of whether activity levels were determined based on only the wake periods preceding the experimental sleep period or on wake periods preceding and following sleep, suggesting that the enhanced dynamics in wake-inactive cells are unrelated to the encoding of information during the prior wake phase.

Wide-field imaging confirmed the more widespread topography of slow oscillations in comparison to spindles, as well as the anterior-to-posterior traveling of slow oscillation-related activity, a feature also reported in other studies using calcium imaging (7) and electrophysiological recordings (e.g., refs. 10, 12, 64, 65). Whether the traveling of the slow oscillation reflects spreading via long-range intracortical excitatory connections, consequently depending on the excitatory–inhibitory balance within cortical columns, or critically involves thalamic regulation is not clear (7, 66, 67). Notably, our wide-field imaging did not show the pronounced increase in Pyr calcium activity during spindles that nested in slow oscillation upstates, compared with solitary spindles, which we revealed with two-photon imaging of the Pyr soma. This discrepancy might be related to the fact that, for the most part, wide-field imaging covered calcium activity of apical dendrites, whose dynamics are expected to differ from those of the soma [e.g., as to the reflection of action potentials (54)].

Although our calcium imaging data mirrored topography and its temporal dynamics for spindles and slow oscillations quite well, correlations between calcium activity of the cells and our electrophysiological amplitude measures, although significant, remained rather modest. This is owing to the fact that calcium signal and EEG amplitude reflect different aspects of activity: on the one hand, calcium level in the contributing neurons and, on the other hand, the synchronized changes in membrane potential mainly of Pyr cells, as the parallel orientation of these neurons and their dendrites enables the summation of extracellular field potentials. It is thus not unexpected that the observed correlations were highest for Pyr activity. The calcium activity in Pyr cells was most robustly associated with the amplitude of slow oscillation that co-occurred with a spindle, underscoring that the up-regulation of calcium activity in these cells is particularly strong when spindles nest in the slow oscillation upstate.

Not only was the size of correlation coefficients between measures of EEG oscillations and calcium activity modest but statistical effect sizes (partial eta-squared) for the observed main effects were also consistently <0.3 despite their high significance ($P < 0.01$). In fact, the overall moderate magnitude of effects agrees well with electrophysiological studies demonstrating that spontaneous firing rates of cortical neurons are log-normally distributed, with the majority of neurons showing very low firing rates [<0.2 Hz (68)] and, importantly, that only a small fraction of these neurons is recruited for the slow oscillation and spindle events of interest here (69–71). Even during events of highly synchronized activity like the upstate of the slow oscillation, no more than 3% of all cells are synchronously active. Concurring with those findings, our calcium imaging approach unselectively covering all cells revealed that changes in calcium activity accompanying slow oscillations and spindles were always conveyed by only a subsample of neurons covered. Thus, our calcium imaging approach corroborates the notion that slow oscillations and spindles are not associated with a global recruitment of neural firing activity but only with activity in distinct neuronal subpopulations, which are possibly those involved in encoding of information during prior wakefulness (72–74).

In the current study, we aimed at linking changes in calcium activity in distinct subsets of cortical neurons to EEG field potential oscillations known to be involved in memory formation during sleep. The basic question arises of to what extent the assessed calcium signal changes relate to action potential activity. Although the fluorescent calcium indicator we used (GCaMP6f) enables the reliable detection of single action potentials (75), it is likely that not all calcium transients detected in our study represent action potentials. However, additional analysis on neuropil-corrected signals excluded the contamination of our measurements with scattered fluorescence from dendrites. Moreover, such

contamination should bias calcium signal levels in the different cell types toward the same direction, which contrasts with our findings of partly opposed changes. Overall, these analyses ensured that the pattern of calcium signal changes coinciding with the EEG oscillations of interest, for the most part, reflect soma-specific events, although this does not exclude the presence of calcium events without spiking. Nevertheless, it seems justified to assume that our measures of soma-specific calcium activity are substantially correlated to cell activity in terms of action potentials (75, 76). However, to precisely characterize this relationship, further experiments are required combining recordings of calcium and electrical activity in single units.

Despite the insights this study provides into the regulation of microcircuits during slow oscillations and sleep spindles, three principle limitations need to be considered. First, compared with electrophysiological detection of firing activity, the temporal resolution of the applied two-photon calcium imaging is rather low, mainly owing to the rather slow decay times of the calcium indicator (in this case, GCaMP6f). Nevertheless, the decay times, together with the 6-Hz frame rate we used in our experiments, are sufficient to cover the EEG oscillatory phenomena of interest [slow oscillation and spindle events (the latter basically defined by their power envelope)], which comprise frequencies <3 Hz. However, our frame rate for two-photon imaging was not sufficient to dissociate changes in calcium activity for subtypes of spindles with faster and slower oscillatory frequency (77) and, importantly, precludes a reliable discrimination of activity changes occurring in synchrony with a specific phase of these oscillations (52, 53). This limitation possibly relates to the seemingly paradoxical observation that during slow oscillation-spindle events, Pyr cell somata show distinct increases in calcium activity in the presence of perisomatic inhibition and presumed hyperpolarization by PV-Ins, which, itself, is expected to decrease calcium activity (78). The increase in calcium activity in Pyr cells during slow oscillation-spindle events likely reflects excitatory inputs (e.g., from thalamocortical projections) occurring during the excitable troughs of the spindle cycle. PV-In activity, on the other hand, with a slight delay, closes the excitatory phase of the spindle cycle to induce perisomatic hyperpolarization of Pyr cells. However, to scrutinize this scenario, further experimentation is required combining recording of calcium and electrical activity in single units.

A second limitation derives from the fact that we focused on the two major types of cortical interneurons, PV-Ins and SOM-Ins. We revealed a unique constellation of activity between these interneurons that characterizes circuit activity during slow oscillation-spindle events, which raises the question of the factors driving this constellation. Here, long-range connections from subcortical (e.g., thalamic) structures, as well as several other types of intracortical interneurons, might play a role (79–81). Vasoactive intestinal polypeptide (VIP)-positive interneurons are a likely candidate to be considered in future studies. Cortical VIP-positive interneurons have been shown to exert disinhibitory control in cortical circuits via action on SOM-In cells and also appear to be involved in the regulation of EEG oscillations (82–84).

A third limitation relates to our focus on activity in layer 2/3, which might differ from activity in other cortical layers. Slow oscillations propagate from layer 5 to more superficial layers (67), and, in this context, a recent study by Seibt et al. (54) complements the present findings by focusing on layer 5 rather than layer 2/3 neurons. Only concentrating on spindles, the study found spindles to be accompanied by increased calcium activity in the apical dendrites of the cells, but not in the cells' soma throughout the cortical column. Against this backdrop, it is conceivable that the increase in calcium signal observed here in the soma of layer 2/3 Pyr cells specifically during spindle nesting in slow oscillation upstates is even more profound in analyses focusing on apical dendrites of layer 5 neurons (54). While our calcium imaging study reveals a distinct pattern of activity in cortical circuits associated with slow oscillations and spindles, it did not include any intervention. Thus, the central question of causality (i.e., to what extent the observed changes in calcium activity characterizing slow oscillation and spindles indeed play a causal role in the regulation of these EEG events) remains to be resolved (47).

Nevertheless, the limitations of our study in no way challenge its main finding (summarized in Fig. 6) that spindles nesting in slow oscillation upstates are marked by a maximal increase in calcium activity of excitatory Pyr cells, which occurs in the presence of strong perisomatic inhibition by PV-Ins and low dendritic inhibition by SOM-Ins. This might optimize local synaptic plasticity underlying the formation of long-term memory in these circuits.

Materials and Methods

Experimental procedures were approved by the local institutions in charge of animal welfare (Regierungspraesidium Tübingen, State of Baden-Wuerttemberg, Germany). Procedures of surgery and recordings followed, in large part, protocols described previously (38). All used resources are summarized in *SI Appendix*, Table S2.

Animals and Surgery. PV-Cre mice [RRID:IMSR_JAX:008069 (85)] and SOM-Cre mice [RRID:IMSR_JAX:013044 (86)] were used for in vivo two-photon calcium imaging. CaMKII-Cre mice [RRID:IMSR_EM:01153 (87)] crossed with Ai95RCL-GCaMP6f mice [RRID:IMSR_JAX:024105 (88)] and C57BL6/J mice were used for wide-field calcium imaging. The mice were housed in groups of up to five mice in temperature-controlled (22 ± 2 °C) and humidity-controlled (45–65%) cages. Experiments were performed during the light (i.e., rest) period of the 12-h/12-h light/dark cycle. Data collection in all mice started 1 h after light onset. All mice were male and older than 8 wk of age. Detailed information about the surgical implantation procedures is provided in *SI Appendix*.

Two-Photon Image Analysis. Lateral motion was corrected in two steps (89). A cross-correlation–based image alignment (Turboreg) was performed, followed by a line-by-line correction using an algorithm based on a hidden Markov model (90). ROIs containing individual neurons were drawn manually, and the pixel values within each ROI were summed to estimate the fluorescence of this neuron. PV-Ins and SOM-Ins were manually detected by

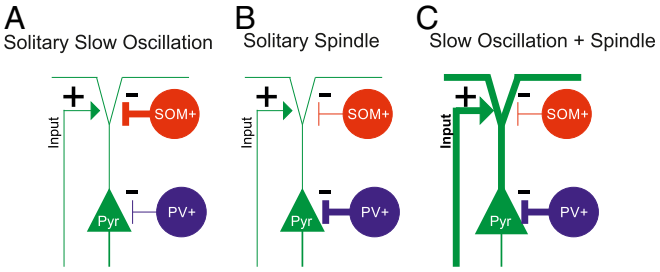

Fig. 6. Schematic illustration of the main findings. Our findings indicate distinct constellations of the excitation/inhibition balance in cortical circuits during slow oscillations and spindles depending on whether these events occur in isolation (Solitary Slow Oscillation, Solitary Spindle) or together, with the spindle nesting in the slow oscillation upstate (Slow Oscillation + Spindle). (*A*) Solitary slow oscillations are hallmarked by increased SOM-In (SOM^+) activity mediating dendritic inhibition of putative Pyr cells at the transition to the downstate and in the initial upstate of the slow oscillation. (*B*) Solitary spindles are hallmarked by increased PV-In (PV^+) activity mediating distinct perisomatic inhibition of Pyr cells in the presence of weak dendritic inhibition by SOM-In cells. (*C*) Spindles nesting in the slow oscillation upstate are hallmarked by a more than threefold increase in Pyr cell activity (compared with respective solitary events), which is possibly driven by specific excitatory inputs to these cells. Simultaneously, Pyr cells receive strong perisomatic inhibition through PV-Ins, while their dendritic inhibition via SOM-Ins is reduced. We speculate that this constellation of excitatory and inhibitory inputs during slow oscillation-spindle events facilitates dendritic synaptic plasticity in Pyr cells underlying memory formation during sleep. The "+" and "−" symbols indicate excitatory–inhibitory inputs, and the thick vs. thin lines indicate the strength of inputs to Pyr cells.

red fluorescence signal expressed by AAV2/1-Flex-tdtomato. Surrounding neurons not expressing tdTomato were considered putative Pyr cells [these cells likely include other types of interneurons, although the proportion of them is negligible (<10%) (80, 91)]. The analyses aimed at globally assessing calcium transients in the cells of interest during solitary EEG slow oscillations, spindles, and slow oscillation-spindle events. For this purpose, the raw fluorescence signal for an individual cell was calculated by averaging the pixel intensity within the respective ROIs for each frame. Subsequently, these values were transformed into ΔF/F values, in which the baseline for each frame and each cell was defined by the corresponding 20th percentile value within a sliding ±3-min window. This procedure simultaneously normalizes and high-pass-filters the signal. The values were then used for statistical testing in all analyses, except if based on neuropil-corrected values. To examine to what extent nonspecific neuropil signal contributed to our results, we performed additional analyses in which the neuropil signal was subtracted from the ΔF/F signal of each individual cell (75, 76) (*SI Appendix*, Fig. S2). The neuropil signal was estimated for each ROI as the average pixel values within a donut-shaped neuropil area, which was defined as a circle (three-pixel radius) around each cell's ROI omitting soma from other cells and the pixels directly adjoining to the cell's soma. The corrected signal was estimated as $\Delta F/F_{cell\_corrected(t)} = \Delta F/F_{cell\_measured} - r \times \Delta F/F_{neuropil}$, where $r = 0.7$ (76).

Wide-Field Image Analysis. To define ROIs for the imaging data from CaMKII-GCaMP6 mice, the area within the window was divided into 36 ROIs (Fig. 4). For each frame, the pixel values within an individual ROI were summed, and this value was then normalized by dividing by the 30th percentile value of all frames of this ROI within a ±3-min interval (f_{norm}). This normalization affects all frames within a 6-min interval in an analogous way [a similar procedure is reported by Tian et al. (92)].

Statistical Analyses. To link calcium signal recordings to the EEG oscillatory phenomena of interest, data from all recordings were baseline-corrected to a common baseline interval, which was the interval 3 to 2 s before the onset of the respective EEG events of interest (i.e., slow oscillations, spindles, slow oscillation-spindle events). For two-photon experiments, calcium signals were baseline-corrected separately for each detected cell. Then, the mean ΔF/F signal was calculated for each frame across all cells. For neuropil-corrected calcium events, event rates (per second) for each cell were likewise first calculated for the baseline interval 3 to 2 s before event onset. Then, mean rates across all cells were calculated. ANOVAs comprising a co-occurring/solitary factor and a phase factor were used to test for significant differences between (co-occurring) slow oscillation-spindle events and solitary slow oscillations and spindles, respectively, and their phases (i.e., transition, up, down, and after phases for comparisons of the slow oscillations and during and after phases for spindle comparisons). Post hoc *t* tests were applied to specify significant main and interaction effects. For the analyses of differences from baseline levels of activity during solitary slow oscillations and spindles and during slow oscillation-spindle events, we used nonparametric permutation tests, as these tests are known to overcome the multiple comparisons problem (93).

Pearson correlations were calculated to assess the relationship between calcium activity and slow oscillation amplitude and spindle power, respectively. Correlations were calculated between the mean ΔF/F signal of all Pyr cells, PV-Ins, and SOM-Ins during the transition, down, up, and after phases and the different slow oscillation amplitude measures (i.e., negative-to-positive peak amplitude, negative half-wave peak amplitude, positive half-wave peak amplitude), separately for solitary slow oscillations and slow oscillation-spindle events. Corresponding correlations were calculated between the mean ΔF/F signal and spindle amplitude. As the amplitude measure during an acute spindle, we used the rms of EEG power (in the 7–15-Hz band) during a spindle, which was normalized for each animal to the average rms signal during all SWS intervals not containing any slow oscillation or spindle (set to 100%). For wide-field imaging experiments, differences from the baseline interval were assessed using nonparametric permutation tests.

ACKNOWLEDGMENTS. We thank Dr. Takashi Sato for helpful advice and general support of the study and Andrea Gall for technical assistance. This study was supported by Deutsche Forschungsgemeinschaft Grant SFB 654 (to J.B.) and the Werner Reichardt Centre for Integrative Neuroscience (CIN) at the Eberhard Karls University of Tübingen. The CIN is an Excellence Cluster within the framework of the Excellence Initiative (EXC 307).

1. Steriade M (2003) The corticothalamic system in sleep. *Front Biosci* 8:d878–d899.
2. Steriade M (1993) Cholinergic blockage of network- and intrinsically generated slow oscillations promotes waking and REM sleep activity patterns in thalamic and cortical neurons. *Prog Brain Res* 98:345–355.
3. Steriade M, Timofeev I, Grenier F (2001) Natural waking and sleep states: A view from inside neocortical neurons. *J Neurophysiol* 85:1969–1985.
4. Volgushev M, Chauvette S, Mukovski M, Timofeev I (2006) Precise long-range synchronization of activity and silence in neocortical neurons during slow-wave oscillations [corrected]. *J Neurosci* 26:5665–5672.
5. Fiáth R, et al. (2016) Laminar analysis of the slow wave activity in the somatosensory cortex of anesthetized rats. *Eur J Neurosci* 44:1935–1951.
6. Steriade M, Nuñez A, Amzica F (1993) Intracellular analysis of relations between the slow (< 1 Hz) neocortical oscillation and other sleep rhythms of the electroencephalogram. *J Neurosci* 13:3266–3283.
7. Stroh A, et al. (2013) Making waves: Initiation and propagation of corticothalamic Ca2+ waves in vivo. *Neuron* 77:1136–1150.
8. Lemieux M, Chen J-Y, Lonjers P, Bazhenov M, Timofeev I (2014) The impact of cortical deafferentation on the neocortical slow oscillation. *J Neurosci* 34:5689–5703.
9. Luczak A, Barthó P, Marguet SL, Buzsáki G, Harris KD (2007) Sequential structure of neocortical spontaneous activity in vivo. *Proc Natl Acad Sci USA* 104:347–352.
10. Massimini M, Huber R, Ferrarelli F, Hill S, Tononi G (2004) The sleep slow oscillation as a traveling wave. *J Neurosci* 24:6862–6870.
11. Olcese U, Esser SK, Tononi G (2010) Sleep and synaptic renormalization: A computational study. *J Neurophysiol* 104:3476–3493.
12. Klinzing JG, et al. (2016) Spindle activity phase-locked to sleep slow oscillations. *Neuroimage* 134:607–616.
13. Mölle M, Born J (2011) Slow oscillations orchestrating fast oscillations and memory consolidation. *Prog Brain Res* 193:93–110.
14. Contreras D, Steriade M (1997) Synchronization of low-frequency rhythms in corticothalamic networks. *Neuroscience* 76:11–24.
15. Timofeev I, Steriade M (1996) Low-frequency rhythms in the thalamus of intact-cortex and decorticated cats. *J Neurophysiol* 76:4152–4168.
16. Lüthi A (2014) Sleep spindles: Where they come from, what they do. *Neuroscientist* 20:243–256.
17. Bonjean M, et al. (2011) Corticothalamic feedback controls sleep spindle duration in vivo. *J Neurosci* 31:9124–9134.
18. De Gennaro L, Ferrara M (2003) Sleep spindles: An overview. *Sleep Med Rev* 7: 423–440.
19. Diekelmann S, Born J (2010) The memory function of sleep. *Nat Rev Neurosci* 11: 114–126.
20. Neske GT (2016) The slow oscillation in cortical and thalamic networks: Mechanisms and functions. *Front Neural Circuits* 9:88.
21. Rasch B, Born J (2013) About sleep's role in memory. *Physiol Rev* 93:681–766.
22. Steriade M, Timofeev I (2003) Neuronal plasticity in thalamocortical networks during sleep and waking oscillations. *Neuron* 37:563–576.
23. Ulrich D (2016) Sleep spindles as facilitators of memory formation and learning. *Neural Plast* 2016:1796715.
24. Tononi G, Cirelli C (2014) Sleep and the price of plasticity: From synaptic and cellular homeostasis to memory consolidation and integration. *Neuron* 81:12–34.
25. Chauvette S, Seigneur J, Timofeev I (2012) Sleep oscillations in the thalamocortical system induce long-term neuronal plasticity. *Neuron* 75:1105–1113.
26. Rosanova M, Ulrich D (2005) Pattern-specific associative long-term potentiation induced by a sleep spindle-related spike train. *J Neurosci* 25:9398–9405.
27. Timofeev I, et al. (2002) Short- and medium-term plasticity associated with augmenting responses in cortical slabs and spindles in intact cortex of cats in vivo. *J Physiol* 542:583–598.
28. Ji D, Wilson MA (2007) Coordinated memory replay in the visual cortex and hippocampus during sleep. *Nat Neurosci* 10:100–107.
29. Ramanathan DS, Gulati T, Ganguly K (2015) Sleep-dependent reactivation of ensembles in motor cortex promotes skill consolidation. *PLoS Biol* 13:e1002263.
30. Rasch B, Büchel C, Gais S, Born J (2007) Odor cues during slow-wave sleep prompt declarative memory consolidation. *Science* 315:1426–1429.
31. Bergmann TO, Mölle M, Diedrichs J, Born J, Siebner HR (2012) Sleep spindle-related reactivation of category-specific cortical regions after learning face-scene associations. *Neuroimage* 59:2733–2742.
32. Clemens Z, et al. (2007) Temporal coupling of parahippocampal ripples, sleep spindles and slow oscillations in humans. *Brain* 130:2868–2878.
33. Staresina BP, et al. (2015) Hierarchical nesting of slow oscillations, spindles and ripples in the human hippocampus during sleep. *Nat Neurosci* 18:1679–1686.
34. Dudai Y, Karni A, Born J (2015) The consolidation and transformation of memory. *Neuron* 88:20–32.
35. Inostroza M, Born J (2013) Sleep for preserving and transforming episodic memory. *Annu Rev Neurosci* 36:79–102.
36. Latchoumane CV, Ngo H-VV, Born J, Shin H-S (2017) Thalamic spindles promote memory formation during sleep through triple phase-locking of cortical, thalamic, and hippocampal rhythms. *Neuron* 95:424–435.e6.
37. Sejnowski TJ, Destexhe A (2000) Why do we sleep? *Brain Res* 886:208–223.
38. Niethard N, et al. (2016) Sleep-stage-specific regulation of cortical excitation and inhibition. *Curr Biol* 26:2739–2749.
39. Grosmark AD, Buzsáki G (2016) Diversity in neural firing dynamics supports both rigid and learned hippocampal sequences. *Science* 351:1440–1443.
40. Watson BO, Levenstein D, Greene JP, Gelinas JN, Buzsáki G (2016) Network homeostasis and state dynamics of neocortical sleep. *Neuron* 90:839–852.

41. Vanni MP, Murphy TH (2014) Mesoscale transcranial spontaneous activity mapping in GCaMP3 transgenic mice reveals extensive reciprocal connections between areas of somatomotor cortex. *J Neurosci* 34:15931–15946.
42. Steriade M (2000) Corticothalamic resonance, states of vigilance and mentation. *Neuroscience* 101:243–276.
43. Mann EO, Kohl MM, Paulsen O (2009) Distinct roles of GABA(A) and GABA(B) receptors in balancing and terminating persistent cortical activity. *J Neurosci* 29:7513–7518.
44. Mayne EW, Craig MT, McBain CJ, Paulsen O (2013) Dopamine suppresses persistent network activity via D(1) -like dopamine receptors in rat medial entorhinal cortex. *Eur J Neurosci* 37:1242–1247.
45. Kuki T, et al. (2015) Contribution of parvalbumin and somatostatin-expressing GABAergic neurons to slow oscillations and the balance in beta-gamma oscillations across cortical layers. *Front Neural Circuits* 9:6.
46. Lemieux M, Chauvette S, Timofeev I (2015) Neocortical inhibitory activities and long-range afferents contribute to the synchronous onset of silent states of the neocortical slow oscillation. *J Neurophysiol* 113:768–779.
47. Funk CM, et al. (2017) Role of somatostatin-positive cortical interneurons in the generation of sleep slow waves. *J Neurosci* 37:9132–9148.
48. Pfeffer CK, Xue M, He M, Huang ZJ, Scanziani M (2013) Inhibition of inhibition in visual cortex: The logic of connections between molecularly distinct interneurons. *Nat Neurosci* 16:1068–1076.
49. Jiang X, et al. (2015) Principles of connectivity among morphologically defined cell types in adult neocortex. *Science* 350:aac9462.
50. Murayama M, et al. (2009) Dendritic encoding of sensory stimuli controlled by deep cortical interneurons. *Nature* 457:1137–1141.
51. Palmer L, Murayama M, Larkum M (2012) Inhibitory regulation of dendritic activity *in vivo*. *Front Neural Circuits* 6:26.
52. Peyrache A, Battaglia FP, Destexhe A (2011) Inhibition recruitment in prefrontal cortex during sleep spindles and gating of hippocampal inputs. *Proc Natl Acad Sci USA* 108:17207–17212.
53. Puig MV, Ushimaru M, Kawaguchi Y (2008) Two distinct activity patterns of fast-spiking interneurons during neocortical UP states. *Proc Natl Acad Sci USA* 105: 8428–8433.
54. Seibt J, et al. (2017) Cortical dendritic activity correlates with spindle-rich oscillations during sleep in rodents. *Nat Commun* 8:684.
55. Chen SX, Kim AN, Peters AJ, Komiyama T (2015) Subtype-specific plasticity of inhibitory circuits in motor cortex during motor learning. *Nat Neurosci* 18:1109–1115.
56. Wolff SBE, et al. (2014) Amygdala interneuron subtypes control fear learning through disinhibition. *Nature* 509:453–458.
57. Ruch S, et al. (2012) Sleep stage II contributes to the consolidation of declarative memories. *Neuropsychologia* 50:2389–2396.
58. Rothschild G, Eban E, Frank LM (2017) A cortical-hippocampal-cortical loop of information processing during memory consolidation. *Nat Neurosci* 20:251–259.
59. Cichon J, Gan W-B (2015) Branch-specific dendritic Ca($^{2+}$) spikes cause persistent synaptic plasticity. *Nature* 520:180–185.
60. Yang G, et al. (2014) Sleep promotes branch-specific formation of dendritic spines after learning. *Science* 344:1173–1178.
61. Niethard N, Burgalossi A, Born J (2017) Plasticity during sleep is linked to specific regulation of cortical circuit activity. *Front Neural Circuits* 11:65.
62. Diering GH, et al. (2017) Homer1a drives homeostatic scaling-down of excitatory synapses during sleep. *Science* 355:511–515.
63. de Vivo L, et al. (2017) Ultrastructural evidence for synaptic scaling across the wake/sleep cycle. *Science* 355:507–510.
64. Cox R, Korjoukov I, de Boer M, Talamini LM (2014) Sound asleep: Processing and retention of slow oscillation phase-targeted stimuli. *PLoS One* 9:e101567.
65. Kim D, Hwang E, Lee M, Sung H, Choi JH (2015) Characterization of topographically specific sleep spindles in mice. *Sleep (Basel)* 38:85–96.
66. Crunelli V, Hughes SW (2010) The slow (<1 Hz) rhythm of non-REM sleep: A dialogue between three cardinal oscillators. *Nat Neurosci* 13:9–17.
67. Sanchez-Vives MV, McCormick DA (2000) Cellular and network mechanisms of rhythmic recurrent activity in neocortex. *Nat Neurosci* 3:1027–1034.
68. Buzsáki G, Mizuseki K (2014) The log-dynamic brain: How skewed distributions affect network operations. *Nat Rev Neurosci* 15:264–278.
69. Cossart R, Aronov D, Yuste R (2003) Attractor dynamics of network UP states in the neocortex. *Nature* 423:283–288.
70. Gardner RJ, Hughes SW, Jones MW (2013) Differential spike timing and phase dynamics of reticular thalamic and prefrontal cortical neuronal populations during sleep spindles. *J Neurosci* 33:18469–18480.
71. Nir Y, et al. (2011) Regional slow waves and spindles in human sleep. *Neuron* 70: 153–169.
72. Chen Z, Wilson MA (2017) Deciphering neural codes of memory during sleep. *Trends Neurosci* 40:260–275.
73. Hanlon EC, Faraguna U, Vyazovskiy VV, Tononi G, Cirelli C (2009) Effects of skilled training on sleep slow wave activity and cortical gene expression in the rat. *Sleep* 32: 719–729.
74. Vyazovskiy VV, Cirelli C, Pfister-Genskow M, Faraguna U, Tononi G (2008) Molecular and electrophysiological evidence for net synaptic potentiation in wake and depression in sleep. *Nat Neurosci* 11:200–208.
75. Chen T-W, et al. (2013) Ultrasensitive fluorescent proteins for imaging neuronal activity. *Nature* 499:295–300.
76. Peron S, Chen TW, Svoboda K (2015) Comprehensive imaging of cortical networks. *Curr Opin Neurobiol* 32:115–123.
77. Ayoub A, et al. (2013) Differential effects on fast and slow spindle activity, and the sleep slow oscillation in humans with carbamazepine and flunarizine to antagonize voltage-dependent Na^+ and Ca^{2+} channel activity. *Sleep (Basel)* 36:905–911.
78. Magee JC, Avery RB, Christie BR, Johnston D (1996) Dihydropyridine-sensitive, voltage-gated Ca2+ channels contribute to the resting intracellular Ca2+ concentration of hippocampal CA1 pyramidal neurons. *J Neurophysiol* 76:3460–3470.
79. Piantoni G, Halgren E, Cash SS (2016) The contribution of thalamocortical core and matrix pathways to sleep spindles. *Neural Plast* 2016:3024342.
80. Meyer HS, et al. (2011) Inhibitory interneurons in a cortical column form hot zones of inhibition in layers 2 and 5A. *Proc Natl Acad Sci USA* 108:16807–16812.
81. Freund TF, Meskenaite V (1992) gamma-Aminobutyric acid-containing basal forebrain neurons innervate inhibitory interneurons in the neocortex. *Proc Natl Acad Sci USA* 89:738–742.
82. Neske GT, Connors BW (2016) Distinct roles of SOM and VIP interneurons during cortical up states. *Front Neural Circuits* 10:52.
83. Pi H-J, et al. (2013) Cortical interneurons that specialize in disinhibitory control. *Nature* 503:521–524.
84. Walker F, et al. (2016) Parvalbumin- and vasoactive intestinal polypeptide-expressing neocortical interneurons impose differential inhibition on Martinotti cells. *Nat Commun* 7:13664.
85. Hippenmeyer S, et al. (2005) A developmental switch in the response of DRG neurons to ETS transcription factor signaling. *PLoS Biol* 3:e159.
86. Taniguchi H, et al. (2011) A resource of Cre driver lines for genetic targeting of GABAergic neurons in cerebral cortex. *Neuron* 71:995–1013, and erratum (2011) 72:1091.
87. Casanova E, et al. (2001) A CamKIIalpha iCre BAC allows brain-specific gene inactivation. *Genesis* 31:37–42.
88. Madisen L, et al. (2015) Transgenic mice for intersectional targeting of neural sensors and effectors with high specificity and performance. *Neuron* 85:942–958.
89. Komiyama T, et al. (2010) Learning-related fine-scale specificity imaged in motor cortex circuits of behaving mice. *Nature* 464:1182–1186.
90. Dombeck DA, Khabbaz AN, Collman F, Adelman TL, Tank DW (2007) Imaging large-scale neural activity with cellular resolution in awake, mobile mice. *Neuron* 56: 43–57.
91. Hofer SB, et al. (2011) Differential connectivity and response dynamics of excitatory and inhibitory neurons in visual cortex. *Nat Neurosci* 14:1045–1052.
92. Tian L, et al. (2009) Imaging neural activity in worms, flies and mice with improved GCaMP calcium indicators. *Nat Methods* 6:875–881.
93. Maris E, Oostenveld R (2007) Nonparametric statistical testing of EEG- and MEG-data. *J Neurosci Methods* 164:177–190.